Anomalous X-ray diffraction study of the AlPdMn icosahedral phase

1994 J. Phys.: Condens. Matter 6 10725

(http://iopscience.iop.org/0953-8984/6/49/015)

J. Phys.: Condens. Matter 6 (1994) 10725–10745. Printed in the UK

Anomalous x-ray diffraction study of the AlPdMn icosahedral phase

M de Boissieu†‡, P Stephens†, M Boudard‡, C Janot§, D L Chapman‖ and M Audier‡

† Physics Department, SUNY, Stony Brook, NY 11794, USA
‡ Laboratoire de Thermodynamique et Physico-chimie Métallurgique, UA CNRS 29, BP 75, 38402 Saint Martin d'Hères Cédex, France
§ Institut Laue Langevin, BP 156, 38042 Grenoble Cédex 9, France
‖ National Synchrotron Light Source, Upton, NY 11973, USA

Received 31 May 1994, in final form 8 August 1994

Abstract. The atomic structure of the perfect AlPdMn icosahedral phase has been studied on a single grain by anomalous x-ray diffraction close to the Pd edge. A method is proposed for relative normalization of the data, in order to extract the partial structure factor F_{Pd} of the Pd atoms. The Pd is found to be very ordered in the six-dimensional description of the quasicrystal, as was previously inferred from x-ray and neutron single-crystal diffraction data. However, a phason Debye–Waller-like term has to be introduced to account for the data. Comparison of the present data set with low-resolution data indicates the existence of diffuse scattering located close to the Bragg reflections whose intensity scales as $[1-\exp(-B_{perp}Q_{perp}^2)]$ as expected from random fluctuations of the atomic surfaces. The average fluctuation is found to be of the order of 1 Å. Moreover the comparison of the data with a spherical model shows that the atomic surface describing Pd atoms is likely to be made of several disjointed pieces.

1. Introduction

The atomic structure of quasicrystals has been the focus of many experiments since the discovery of the 'perfect' quasicrystal in the AlCuFe and AlPdMn systems [1–4]. These quasicrystals have very sharp Bragg peaks [5, 6] and can be grown as centimetre size grains in the AlPdMn system [6–8]. The quality of these large grains is such that dynamical diffraction can take place on a microscopic scale. In particular the Bormann effect, normally associated with crystals of high perfection, was experimentally shown to occur on a single grain of AlPdMn [9].

The most fruitful approach to the quasicrystal structure determination so far has been through the use of the so called 'high-dimensional' description of quasicrystals (for a recent introduction to the subject see [10]). In this scheme the periodicity is recovered in a six-dimensional space for structures presenting icosahedral symmetry. The periodic space decomposes into two subspaces: E_{par}, the physical space, and E_{perp} the complementary space. The periodic lattice is decorated with three-dimensional objects called atomic surfaces and lying in the perpendicular space. The physical (three-dimensional) structure is obtained by a cut through the periodic decorated lattice. This leads to a factorization of the reciprocal lattice into Q_{par}, the physical momentum which governs the condition for constructive Bragg interference, and Q_{perp}, which governs the intensity of each Bragg peak through the Fourier transform of the atomic surfaces. Any given Bragg peak is indexed by six integers, from

0953-8984/94/4910725+21$19.50

which Q_{par} and Q_{perp} are uniquely defined. Six-dimensional Patterson analysis, obtained by a Fourier transform of the measured intensities, provides some insight into the atomic structure. Experimentally, significant progress may be made in determining the atomic structure if the contributions of different chemical species may be separated by contrast variation [11–13].

Surprisingly, ten years after the discovery of quasicrystals [14], and despite intensive efforts, no model has yet achieved an agreement with data comparable with what is customary in 3D crystallography. Crudely speaking one can say that there is a relatively good agreement with 'poor quality data' (i.e. corresponding to samples containing a large number of phason strain defects (defined below), for instance i-AlLiCu [13, 15, 16]) and a bad agreement with good-quality data (as is the case with 'perfect' icosahedral AlCuFe and AlPdMn i phases). Indeed most of the models fit relatively well the low-Q_{perp} data but are far from reproducing the high-Q_{perp} data, which are mainly sensitive to the details of the atomic structure. This means that all models still are low-resolution models, where the term 'low resolution' refers to the perpendicular space where atomic surfaces are confined. The consequence is that all models will have a common 'hard core', details of the atomic surfaces remaining to be specified. This implies that probably 80% of the atoms are correctly placed but the remaining 20% still have to be specified [17]. In principle, the task to be fulfilled is not so large: at most 400–1000 independent reflections have to be reproduced. The difficulty in accomplishing this job raises the problem of the modelling of quasicrystalline atomic structure and questions the validity of the hypotheses used in the modelling process.

Because of their non-periodic symmetry, quasicrystals have additional degrees of freedom called phasons. The name phason was coined by reference to modulated structures. The free energy of a quasicrystal may be expanded as a functional of the mass density. Because of the periodicity in 6D space there are six phases in each term of this expansion, corresponding to translations of the cut in E_{par} (phonons) and E_{perp} (phasons) [18–21]. Because of the way that the phason degrees of freedom govern atomic positions in a quasicrystal, phasons are not propagative modes. Starting with an idealized quasicrystal, a rigid translation of the cut surface rearranges some of the atoms, but yields a macroscopically indistinguishable quasicrystal. However, localized distortions of the cut surface will create atomic rearrangement, by so-called phason jumps. In the simplest case, an atom will jump from one site to another one close by (for instance at a distance of 1 Å for Al atoms in the AlPdMn case), creating a phason defect. Both sites have almost the same local environment, and thus a very similar energy, but only one is occupied in a perfect quasicrystal.

Phason disorder has been used with various meanings, and so we shall specify briefly our use of this concept. Depending on the correlation between the phason defects, two degrees of disorder can be distinguished. On one hand the defects are introduced through a slope change of the cut, which is equivalent to a shear strain in E_{perp} or phason strain. A uniform shear strain of the 6D lattice results in correlated phason jumps, and to a displacement of the Bragg reflections from their ideal positions. If the sample contains a uniform distribution of shear strain, this will result in the broadening of diffraction peaks scaling with Q_{perp} [22]. Indeed such broadening was observed in all samples before the discovery of 'perfect' quasicrystals [22, 23]. On the other hand, one can introduce phason defects by a random fluctuation of the atomic surfaces in E_{perp}. If the fluctuations are bounded, they will not destroy the delta function Bragg reflections; in this case the long-range quasiperiodic order is preserved [24, 25].

Atomic models for quasicrystals fall into two families: idealized quasicrystalline long-range order and random tiling. Both models predict sharp Bragg diffraction peaks, but differ

in the degree of disorder. It is important to emphasize that these are the extremes which bound a continuum, rather than specifying a dichotomy.

Specifying an ideal quasicrystal model is *a priori* a very difficult task, since in principle an infinite number of parameters are necessary to model the atomic surfaces. A number of supplementary constraints have thus been introduced. The simplest one comes from atomic density and chemical composition, which will govern the overall volume of the atomic surfaces. Another constraint was proposed recently, and concerns the connectivity of the atomic surfaces [26, 27]. This constraint is related to the possibility of atomic phason jumps. Imposing the condition that the matching of certain unit cells should be defined by local rules, such as a Penrose tiling, Katz and co-workers derived a set of ten atomic surfaces which should be used for modelling [28]. These atomic surfaces are faceted objects, bounded by twofold planes, and have been used for the modelling of the perfect i-AlCuFe phase [28, 29]. One should note however that such a restriction is already very severe. There are several examples of tilings which are ideal quasicrystals, and which cannot be described by atomic surfaces with simple boundaries. For instance the 12-fold tiling of the plane with squares and triangles, which is obtained by inflation constructions, has an atomic surface whose border is fractal [30–32].

The random tiling viewpoint abandons the requirement of matching rules to impose quasiperiodicity. Given a set of tiles, one considers all of the different configurations that will tile the 3D space, and gives them an equal weight [33–36]. The fact that any configuration can be accessed via phason jumps implies that the random tiling corresponds to a high-temperature limit. Because no energy is given to the matching of tiles, there is only an entropy term arising from the different possible configurations. The statistics of such an ensemble has been studied numerically and theoretically [35, 37–45]. The main results are (i) the average slope of the cut space is the one of the icosahedral phase (i.e. the long-range quasiperiodic order is maintained; (ii) the entropy of the system varies as the squared gradient of the phason strain. The consequence of such a dependence for 3D systems is that the random tiling is well approximated by an ideal quasicrystal with bounded random fluctuations of the atomic surfaces. This does not destroy the Bragg reflections, but produces an intensity decrease, with a perpendicular Debye–Waller term, together with the appearance of diffuse scattering located close to the Bragg reflections [42, 46]. Note that, analytically, the situation is completely analogous to the case of thermal vibrations. Because of the fluctuations of the atomic surfaces in perpendicular space, they might be viewed, in an average picture, as atomic surfaces with smooth boundaries.

Henley proposed three years ago a set of four tiles called a 'canonical cell' [34], designed to induce a high connectivity of icosahedral atomic clusters. It is believed that the packing fraction of icosahedral clusters will be higher with a random packing of such cells than with an ideal quasicrystal model. Such cells have been used to generate a large-unit-cell approximant modelling different icosahedral quasicrystals [47, 48]. Note that, up to now, no ideal quasicrystal model built up with these four tiles has been discovered, but it is conjectured that the shape of the atomic surface is made of several disconnected pieces, possibly fractal as is the case for the square and triangle tiling. Such a complex shape is directly related to the atomic density, which is higher in these tilings [34, 47, 48].

Ideal quasicrystal and random tiling have frequently been viewed as opposite limits, i.e., energetic against entropic quasicrystal. However, even if the ground state of a 3D system is a quasicrystal, there exists a critical temperature above which the system enters a random tiling type phase or 'unlocked' phase, i.e. the entropy of the system varies as the squared gradient of the phason strain. Below the critical temperature there are isolated phason defects and the quasicrystal is referred as being in a 'locked' phase [35]. This behaviour

was conjectured by Tang and Jaric, Henley and Kalugin [35, 43, 49] and has been verified recently numerically on a Penrose tiling model [50, 51]. The transition temperature is of the order of the energy associated with a matching rule violation. What can we expect for real quasicrystals? The matching rule violation is certainly of very low energy cost and some upper bound can be evaluated. It was observed in the AlCuFe system that a phase transition between a microcrystalline state and a perfect quasicrystal occurs around 650 °C [52–54]. This phase transition obviously involves phason jumps. In the same system Coddens *et al* obtained experimental evidence for the existence of atomic jumps in the perfect quasicrystalline state when the temperature is higher than 650 °C [55, 56]. Above 800 °C the mechanical properties of the icosahedral AlPdMn phase studied on a single grain dramatically change: it goes from a fragile regime to a superplastic one [8, 57]. This might be the result of a high diffusion rate assisted by a phason jump as postulated theoretically by Kalugin and Katz [58]. Finally phason strain disorder present in AlCuFe or AlPdMn quasicrystalline samples obtained by rapid quenching is annealed rapidly when the temperature is higher than 650 °C. All these results strongly suggest that the energy cost for a matching rule violation is probably quite low so that in the high-temperature range (above 700 °C), a real AlCuFe or AlPdMn quasicrystal is likely in an 'unlocked phase' . Even though phason diffuse scattering has not been directly observed, it is of interest to look look for evidence of random phason fluctuations in the Bragg peak intensities.

This paper presents the results of an x-ray diffraction experiment carried out at the Pd x-ray absorption edge on a single grain of the $Al_{68.7}Pd_{21.6}Mn_{9.7}$ icosahedral phase. Using the anomalous scattering amplitude of Pd near its x-ray absorption edge, we have extracted a reliable partial structure factor for the Pd atom alone. Furthermore, by comparing the present high-resolution synchrotron measurements with previous data taken with a x-ray laboratory source, we have found evidence for a phason dependent diffuse scattering. The results of this experiment have been briefly described in a previous communication [59].

Previous contrast variation measurements and simultaneous analysis of single-crystal x-ray and neutron diffraction data allowed the formulation of a low-resolution image (in E_{perp}) of the atomic structure [60, 61]. We will refer to this as the SP (for spherical) model, and it is sketched in figure 1. The reciprocal 6D lattice is a BCC one, corresponding to an FCC direct lattice. As previously shown [62], this 6D FCC lattice may be described as resulting from a supercell on a primitive lattice with translation vector $a = 6.451$ Å (figure 1(a)). The six icosahedral indexes $\{n_i\}$ are then either all integers, producing a family of primitive (P) reflections, or all half-integers, producing the superlattice (S) reflections. The observation that the P reflections are generally stronger than the S reflections emphasizes the naturalness of this division.

In the SP model, the atomic surfaces are modelled by spheres and spherical shells in the E_{perp} direction, located on three special positions of the (doubled) six-cube unit cell (figure 1):

(i) Three successive shells are located on $n_0 = [000000]$: a spherical core of Mn (radius $0.83a$), surrounded by an intermediate shell of Pd (extending up to $1.26a$) and an outer shell of Al (up to $1.55a$).

(ii) On $n_1 = [100000]$, we find a core of Mn (radius $0.52a$) surrounded by a shell of Al (up to $1.64a$).

(iii) A ball of Pd ($0.71a$) is located at the $bc_1 = 1/2[11111\bar{1}]$ position.

Note that only the sites n_0 and bc_1 are occupied by Pd atoms. This strong chemical ordering produces the FCC centring of the lattice. In 3D, this results in a quasiperiodic packing of two types of Mackay icosahedron, each one with a different chemical decoration.

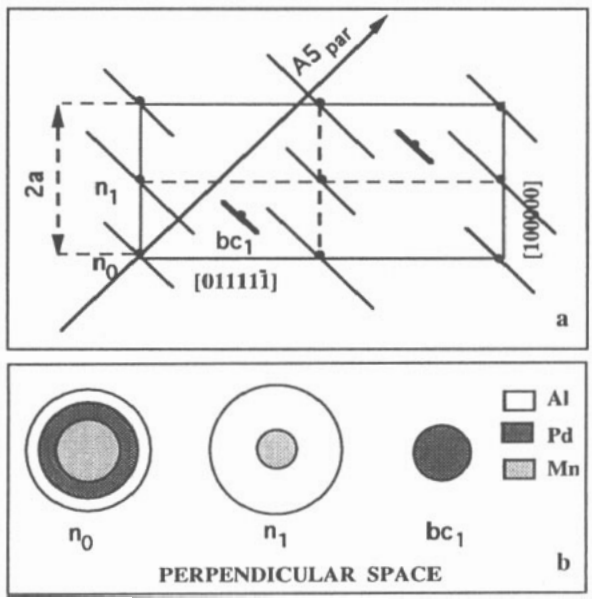

Figure 1. Illustration of the structure of the i-AlPdMn phase. (a) Section of the 6D superspace containing fivefold axes in E_{par} and E_{perp}. The true unit cell has a parameter equal to $2a$ and corresponds to an FCC lattice (solid line). The structure can be described as resulting from a superstructure on a lattice with parameter a (dashed line). Three sites have to be considered: n_0, n_1 and bc_1. The atomic surfaces in n_0 and n_1 are different leading to an FCC lattice. (b) Sketch illustrating the size of the different atomic surfaces in E_{perp} that define the SP model.

A knowledge of the precise shape of the atomic surfaces which describe the Pd atomic position is certainly an important step towards a finer understanding of the atomic structure of quasicrystals. Since all these atomic surfaces are in close contact their shapes are interrelated. In order to proceed to a more detailed description, it is very useful to seek information on a single atomic species. Working close to the Pd x-ray absorption edge allows us to gain information on the Pd sublattice.

The paper is organized as follows: section 2 presents details on the procedure used to extract the partial Pd structure factor; section 3 presents the experimental results with emphasis on the data analysis. For the first time the Pd partial structure factor has been extracted. Those readers mainly interested by the results on the atomic structure can jump directly to section 4 where the comparison with the SP model is presented. The strong chemical order previously inferred from x-ray diffraction experiment is confirmed. However a perpendicular Debye–Waller factor has to be introduced to fully account for the data. In section 5 we show the existence of a diffuse scattering located close to the Bragg reflections, whose intensity scales with $[1-\exp(-B_{perp}Q_{perp}^2)]$, in comparing the present measurements with measurements which integrate over the diffuse scattering. This is a good indication that random fluctuations of the atomic surfaces exist in the perfect AlPdMn icosahedral phase. Moreover, a comparison of the obtained partial structure factor with the SP model indicates that the atomic surfaces are likely to be formed of several disjointed pieces. Implications for the quasicrystal modelling are discussed.

2. Partial structure factor extraction

When tuning the energy of an x-ray beam close to an absorption edge, anomalous scattering

effects take place. The atomic scattering form factor is written

$$f = f_0 + f' + \mathrm{i}f''$$

where f_0 is the usual x-ray atomic form factor, dependent on scattering wave vector, and f' and f'' depend on the x-ray wavelength, but not on scattering angle. f' is in phase with f_0, whereas f'' presents a $\pi/2$ phase difference with f_0 (imaginary component).

The usual procedure when such an experiment is carried out, in biocrystallography or crystallography, is to measure a set of data at two or three different energies and, combined with direct methods, to refine a model with a few reasonable free parameters [63]. Such methods are not yet available for quasicrystal structure determination and one would like to extract the partial structure factor corresponding to the Pd atoms. If a structure factor is measured for two different energies E_1 and E_2 of the incoming x-ray beam, then the partial structure factor of the Pd, F_{Pd}, can be extracted. In effect one can write

$$|F_1| = |F_0 + f_1' F_{\mathrm{Pd}} + \mathrm{i}f_1'' F_{\mathrm{Pd}}| \tag{1}$$

$$|F_2| = |F_0 + f_2' F_{\mathrm{Pd}} + \mathrm{i}f_2'' F_{\mathrm{Pd}}| \tag{2}$$

$$F_0(Q) = f_{\mathrm{Al}}(Q)F_{\mathrm{Al}} + f_{\mathrm{Mn}}(Q)F_{\mathrm{Mn}} + f_{\mathrm{Pd}}(Q)F_{\mathrm{Pd}} \tag{3}$$

where the structure factor F_0 is a constant which does not depend on the x-ray energy, and f_{Al}, f_{Mn} and f_{Pd} are the x-ray atomic form factors. When working below the absorption edge, the variation of f'' may be neglected, and the corresponding term in (1) and (2) can be included in F_0. Moreover it has been shown previously that to a good approximation the quasicrystal structure can be considered as centrosymmetrical [64]. (Note that multiple-scattering experiments performed on similar samples indicate a weak deviation from centrosymmetry [65, 66]. However an intermediate-energy measurement showed that the centrosymmetric hypothesis is justified, see subsection 3.3). Since f'' is a small quantity, one can consider that F_0 and F_{Pd} are either in phase or in opposition. In other words these two quantities are real numbers with only a + or − sign. Finally, because the contrast variation is weak, one can assume that F_1 and F_2 have the same sign. With all the above hypotheses, and if both sets of data are on the same relative scale, a simple difference between $|F_1|$ and $|F_2|$ will give the amplitude of the partial structure of the Pd. Note that the obtained partial structure factor is similar to the one obtained with neutron scattering, without the usual Q-dependent atomic form factor.

One experimental difficulty in this procedure is the relative rescaling of both sets of data. Since the expected intensity variation is small, one must find a way of rescaling data with a very good accuracy. When variation is large enough, measuring at four different contrasts allows one to get the scale factor from a fitting procedure [67]. However, anomalous x-ray contrast is weak, and this technique cannot be employed here. Because we are working with a small sample, bathing in a larger beam, direct rescaling techniques, such as the one employed for diffuse scattering measurement, are difficult to work out [68]. We thus have used another method for data rescaling. The crude SP model is known to reproduce quite well the low-Q_{Perp} data, corresponding to strongest reflections. This is because in the low-Q_{Perp} region, the Fourier transform of the atomic surfaces is mainly sensitive to their size, and not to their precise shape. We have thus compared the 30 low-Q_{Perp} reflections ($Q_{\mathrm{Perp}} < 0.4$ Å^{-1}) of both data sets to the SP model taking into account the f' value at the working energy. In this procedure the only free parameters are a scale factor and a parallel Debye–Waller factor, which allows us to put on the same relative scale both sets of data. An important consistency check is described below in subsection 3.3.

3. Experimental details

A single grain was extracted from the upper part of a Bridgman ingot. It is a 'perfect' icosahedral phase, with a composition $Al_{68.7}Pd_{21.6}Mn_{9.7}$. The sample was ground into a spherical shape, with a diameter of 200 μm, and glued on the tip of a glass fibre. Data collection was carried out at the X3A2 beam line of the National Synchrotron Light Source, Brookhaven. An Si(220) double monochromator selected the incident energy of the unfocused beam. The sample consisted of two domains with a 0.08° misorientation, each one with a mosaic spread of about 0.03° (figure 2(a)). Two sets of data were taken at 20 eV and 1390 eV below the Pd edge (24 350 eV). The values of the anomalous scattering coefficients were obtained from a Kramers–Kronig transform of the fluorescence spectrum measured through the Pd edge. At an energy of 24 330 eV, f' and f'' are -6.5 and 0.8 respectively. These values are equal to -2.5 and 0.5 at 22 960 eV. The contrast is of -4 electrons to be compared to $f(0) = 46$ electrons for Pd.

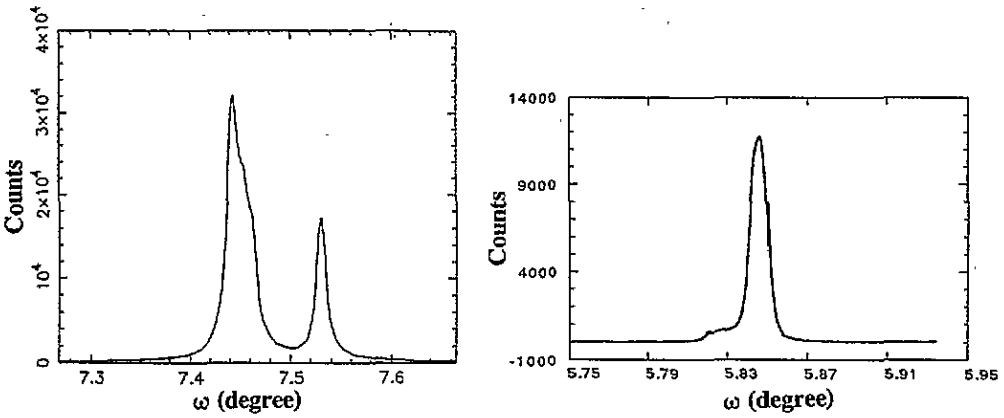

Figure 2. Typical ω-scans used for data collection. (a) Spherically ground sample. There are two grains, each one with a narrow mosaic. Note the tails of the Bragg reflections, which are caused by the surface damage induced by the grinding. (b) Unground sample. Note that the ω-range is half as large as in (a). There are no longer any tails.

3.1. Monitoring of the intensity

Special care has to be taken when measuring intensity on a synchrotron x-ray source, especially when using a small sample. This is because of beam intensity and position fluctuations and inhomogeneity. As a result, standard normalization with a total flux monitor (ion chamber) is in general not sufficient. We present in the following section a few of the standard tests, which allow us to evaluate the accuracy of the measured intensity.

The absorption length is calculated to be 0.45 and 0.40 cm^{-1} close to and away from the edge respectively. With the spherical sample used, this will correspond to an attenuation factor of about 1.9, almost independent of the scattering angle. This small attenuation is indeed a crucial point, for expected intensity variations are small, and high accuracy is needed for their measurement. A ψ scan, in which the sample is rotated around the scattering vector, showed very little intensity variation, the statistical standard deviation being of the order of 1.5%.

The integrated intensity of 330 reflections in the range $Q_{par} = 0$–11 Å^{-1} and $Q_{perp} = 0$–1 Å^{-1} was measured by performing ω-scans. Each peak was first precentred in ω. A subset of 32 weak reflections in the Q_{perp} range 1–1.3 Å^{-1} were measured with a triple counting time.

To get rid of any beam fluctuation, a standard reflection was measured every 30 min. Indeed on a time scale of the order of a few hours, significant variations of the order of 5% were noticed. However, the intensity variation was found to be smooth, so that a simple linear interpolation of the scaling factor between two standards was accurate enough. The reliability of this kind of rescaling was checked by measuring the same subset of reflections several times. The agreement was found to be better than 1%. This shows that the reproducibility of the measurement is very good.

All reflections were measured in the same asymmetric unit. For a few of them, all of the accessible equivalent reflections have been measured. After renormalization, variation of symmetry-equivalent intensities were found to be of the order of 1% for weak reflections and 4% for stronger ones, probably to be related to the profile of the ω-scan which changes (the two grains have a different relative orientation).

Finally, to insure a good energy stability below the edge, where the f' variation with energy is very steep, an energy calibration was performed every 3 h. The resulting energy stability was found to be about 4 eV, corresponding to an f' variation of 0.2 electron.

3.2. Integrated intensity measurement

A well known problem with grinding is the introduction of surface strain on the sample [69]. This results in long wings extending far away from the Bragg peak in a mosaic effect (figure 2(a)), with the wings extending to the order of $\pm 1°$ in transverse or ω-scans, but not for radial scans. It is impractical to perform the integration on such a large range. All ω-scans were performed with a 0.4° full width in 0.002° steps. In doing this a portion of the Bragg intensity is not integrated, the intensity left in the wings being 15% of the total intensity. We have checked on a few reflections that the intensity left in the tails indeed is proportional to the total intensity, and does not depend on any other parameter. As a result and since all peaks were measured in the same way (i.e. with the same centring), the integration can be performed in a simple way by subtracting a constant background measured with 20 points on each side of the scan.

In order to check that the grinding does not affect the obtained result, the same experiment has been repeated on an unground sample taken from the same Bridgman-grown ingot. It had roughly the form of a tetrahedron, with edges ~ 0.2 mm. The sample consists of a main crystallite, with a very sharp mosaic (0.01°), and two or three small companions, 10% in volume (figure 2(b)). Comparing figures 2(a) and (b), it is obvious that this unground sample does not present the tails characteristic of the surface damage, so that now all the intensity is integrated. About 120 reflections were collected on the X17 high-energy wiggler beam line at the two energies 20 eV and 1390 eV below the Pd edge, with a double Laue Si[220] monochromator. To our initial surprise, the intensity at 24 keV from the wiggler line was comparable to what we obtained at the X3 bending magnet. In fact, this is somewhat below the energy range of the x-ray optical design of that beam line. Specifically, it has graphite filters to absorb the relatively low-energy part of the spectrum, and its 0.7 mm thick Si(111) crystal in Laue (transmission) geometry has a limited efficiency at 24 keV.

We took care to cover the entire range of Q_{perp} in these comparisons, since the high-Q_{perp} reflections are the most sensitive to any phason disorder. Due to the very irregular shape of the single grain, no absorption correction has been carried out. However, the

situation is not very serious, because the asymmetric unit of the icosahedron is small, so the relative movement of the sample during the measurement is restricted. Moreover the absorption is small at these energies.

Surprisingly enough, both sets of data (spherical sample and unground sample) did agree very well. For the two energies, the weighted R factor, defined as $[[\sum(1/\sigma^2_{obs})(I_{obs} - I_{cal})^2]/\sum(1/\sigma^2_{obs})I^2_{obs}]^{1/2}$, calculated when comparing the two data sets, is 0.04 . Because of the very good quality of the unground sample, the three strongest reflections were clearly affected by extinction. Their intensities, when compared to the spherical sample data set, are significantly smaller (as large as 25% for the strongest reflection). The intensity difference is directly related to the value of the structure factor, which is a signature that indeed dynamical diffraction is taking place. As a consequence, this allows us to put some limit on the effect of extinction on the other integrated intensity measurements. In particular, this shows that the data obtained with the spherical sample are not affected by any extinction.

The Pd partial structure factor extracted from the unground sample showed exactly the same behaviour as the one obtained with the spherical sample: all the conclusions discussed in the following sections were found to be strictly identical. This clearly demonstrates that the spherical grinding does not introduce any errors in the measurement of integrated intensities. In the following all results presented concern data taken with the spherically ground sample.

3.3. Consistency check

As an internal consistency check, and to verify the important hypotheses of centrosymmetry, same sign for F_1 and F_2, and weak variation of f'', a subset of 100 reflections was measured at an intermediate energy of 24 203 eV, where $f' = -4.5$. If the relative normalization and other hypotheses are correct, the normalized structure factor should follow a linear variation with f'. Let us define ΔF_1 and ΔF_2 as follows:

$$\Delta F_1(Q) = |F_{check}(Q)| - |F_1(Q)| \tag{4}$$

$$\Delta F_2(Q) = |F_{check}(Q)| - |F_2(Q)| \tag{5}$$

where F_1, F_{check}, and F_2 stand for the normalized structure factor at 22 960, 24 203, and 24 330 eV respectively. Since $f' = -2.5$, -4.5, and -6.5 at these energies, one should have $\Delta F_1 = -\Delta F_2$. This is indeed what was observed experimentally as shown in figure 3, where the ratio $\Delta F_1/\Delta F_2$ is represented. A statistical analysis of this ratio shows that the average value of the ratio is 0.99 with a standard deviation of 0.2, the data ensemble having an almost Gaussian distribution, which is an indication that errors are random and that no large systematic errors were introduced during the procedure. From this, one can deduce that the standard deviation of the partial Pd structure factor is well accounted for if the standard deviation of each measured intensity is expressed as

$$\sigma^2 = \sigma^2_{Poiss} + \alpha^2 I^2 \tag{6}$$

where σ_{Poiss} is the standard deviation obtained by the counting statistics and α is a constant equal to 0.02, i.e. errors on the intensity measurement are equal to 2% for strong reflections. This α term accounts for the reproducibility of the measurement. Propagating this error leads to the standard deviation in F_{Pd} called σ_2 in table 1. Note that the relative error is larger for P reflections where the intensity variation is smaller.

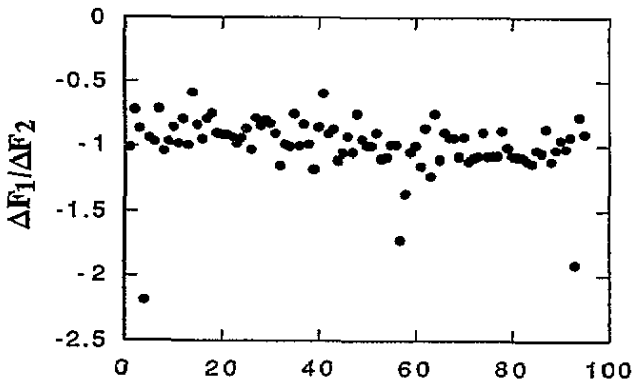

Figure 3. Variation of the ratio $\Delta F_1/\Delta F_2$ using data collected at three different energies (see text). If the rescaling procedure is correct this ratio should be unity, within statistical errors.

Table 1. Results for the selected reflections shown figure 4. N and M are the reflection indices defined by Cahn *et al* [70], Mul is the reflection multiplicity, Q_{par} and Q_{perp} are the parallel and perpendicular wave vectors. I_1 and I_2 are the normalized intensities measured at 1390 and 20 eV below the Pd edge, corresponding to an f' value equal to -2.5 and -6.5 respectively. F_{Pd} is the partial Pd structure factor extracted from the normalized intensity. σ_1 is the standard deviation in F_{Pd}, obtained when only the counting statistic is taken into account. σ_2 is obtained by adding a 2% fluctuation on each measured intensity (see text and expression (6)). Data for all 330 reflections are available from the authors.

	N	M	Mul	Q_{par}	Q_{perp}	I_1	I_2	F_{Pd}	σ_1	σ_2
A	18	29	12	2.990	0.170	1 946 600	1 865 000	29.5	2.1	19.6
B	20	32	30	3.150	0.280	1 253 392	1 089 000	76.0	2.2	15.5
C	52	84	30	5.100	0.180	1 736 390	1 441 000	117.3	2.7	18.0
D	102	165	20	7.140	0.090	773 311	647 600	74.6	3.2	12.3
E	70	113	60	5.910	0.240	434 441	369 400	51.3	1.9	9.2
F	104	168	60	7.210	0.250	405 701	315 500	75.3	2.1	8.8
G	136	220	30	8.240	0.110	738 223	568 700	105.1	2.2	11.6
H	188	304	12	9.690	0.210	289 541	191 200	100.8	2.4	7.3
I	188	304	60	9.690	0.210	249 220	171 900	84.6	2.4	6.9
J	15	24	20	2.730	0.250	63 922	37 620	58.9	1.3	3.4
K	47	76	12	4.850	0.100	60 533	21 610	99.0	1.7	3.3
L	91	147	60	6.740	0.230	109 983	55 210	96.7	2.0	4.5
M	123	199	12	7.840	0.060	123 967	51 410	125.4	2.1	4.7
N	175	283	60	9.350	0.190	65 020	27 960	87.8	2.4	3.9
O	195	315	60	9.870	0.340	35 234	18 650	51.1	2.0	2.4
P	195	315	20	9.870	0.340	17 913	10 080	33.4	2.0	3.1
Q	79	127	60	6.270	0.430	43 530	30 950	32.7	0.9	2.6
R	79	127	60	6.270	0.430	11 024	7036	21.1	0.8	1.6

4. Atomic structure of Pd

As explained in section 2, the data taken at two different energies were put on the same relative scale after comparison of the 30 low-Q_{perp} peaks with the SP model. The only fitted parameters were a scale factor and an overall parallel Debye–Waller factor which was found to be equal to 0.0044 Å^2 in both cases. Introducing the anomalous correction, an R factor of 0.05 was obtained for the agreement between the two subsets of data. This scale factor is then applied to the remaining data (300 reflections), and the partial Pd structure factor is

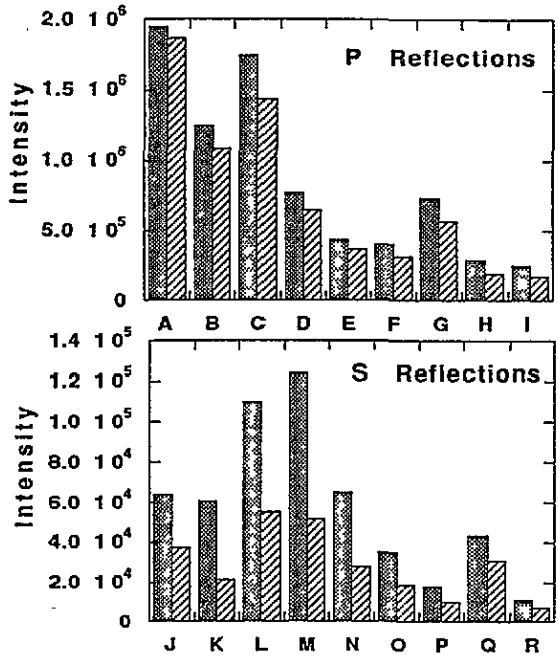

Figure 4. Comparison of a few integrated intensities after relative rescaling. Dark and light boxes correspond to measurement at −1390 eV and −20 eV respectively. The top panel corresponds to P reflections, the bottom one to S reflections (see text). Intensity variation is generally greater for S reflections.

extracted from the difference between the two rescaled data sets.

A few of the rescaled data are presented in table 1 and figure 4. Recall that the reciprocal lattice is body-centred icosahedral. Reflections fall then in two classes: primitive reflections (P), with all integer indices, and superstructure reflections (S), with all half-integer indices. When expressed with the N and M indices [28, 70] the S reflections have N odd, and the P reflections have N even. As might be expected the intensity variation is generally stronger for superstructure reflections. Since the chemical ordering is essentially due to Pd, S-type reflections are expected to present a stronger variation when the energy is tuned close to the Pd edge. As can be seen in figure 4, this is indeed the case, and variations as large as 50% are observed. Note the importance of working with a single grain instead of a powder. Degenerate reflections like O and P would have been attributed an equal weight in a powder experiment, which is obviously not the case.

According to the SP model, the Pd is located on only the sites n_0 and bc_1 in the 6-cube. Indeed a 6D Patterson analysis of the data, obtained by a Fourier transform of the square of the partial Pd structure factor, shows correlation only in n_0 and bc_1, which is a confirmation of the Pd ordering. Figure 5 presents a rational cut of the 6D Patterson map in a plane containing a fivefold axis in both $E_{\parallel}$ and $E_{\perp}$. The primitive unit cell is outlined. Only contributions in n_0 and bc_1 have a significant intensity.

This result can also be found looking at the $Q_{\perp}$ dependence of the Pd structure factor, once it is corrected for the parallel Debye–Waller factor. Since there is Pd in only two sites, the structure factor is written

$$F_{\mathrm{Pd}} = G_1(Q_{\perp}) + G_2(Q_{\perp}) \exp(\mathrm{i}Q \cdot R) \tag{7}$$

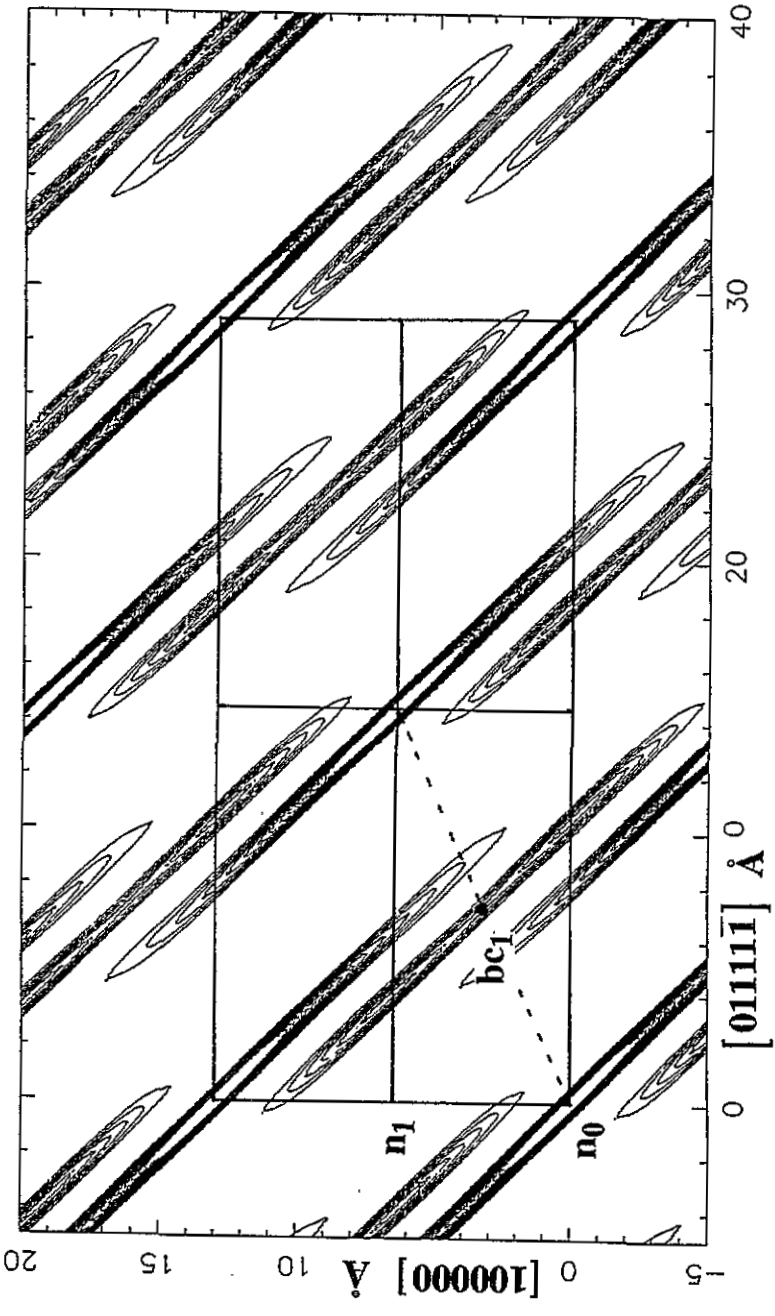

Figure 5. Rational cut of the 6D Patterson map in a plane containing a fivefold axis in both parallel and perpendicular space. The primitive unit cell is outlined. Only contributions at n_0 and bc_1 have a significant intensity.

where $G_1(Q_{perp})$ and $G_2(Q_{perp})$ are the Fourier transforms of the atomic surfaces located in n_0 and bc_1, and $R = 0.5[111111]$. The phase factor $\exp(iQ \cdot R)$ is real and can only take the value $+1$ or -1 depending only on the parity of the sum of the six indices. When expressed with the N and M indices [70] this phase factor is $+1$ when N and M have the same parity and -1 when N and M have opposite parity. This Q_{Perp} dependence is shown in figure 6, where the two families of indices have been separated, and the partial structure factors have been corrected for a single parallel Debye–Waller factor equal to 0.0044 Å^2.

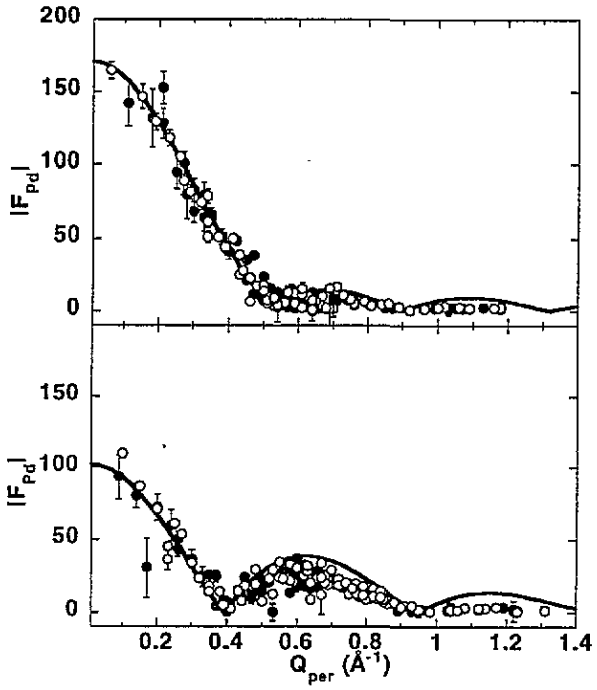

Figure 6. Q_{perp} dependence of the partial structure factor F_{Pd} extracted from the data. The partial structure factor is corrected for a parallel Debye–Waller term. Upper panel corresponds to reflections having N and M the same parity and lower panel to reflections with N and M having different parity. In both cases, the filled (open) circles are the P (S) reflections having N even (odd). The solid line corresponds to the calculation with the SP model.

In the general case, the interference between the different atomic surfaces produces four families of reflections based on the parity of N and M [28]. However, since Pd atoms are found only at n_0 and bc_1, these collapse to two families, depending on the phase factor defined above. In particular each family contains reflections labelled P and S (see section 1). As shown in figure 6 all data points fall only on two curves as expected from expression (7). This clearly demonstrates the strong Pd chemical order. In the SP model, G_1 and G_2 depend only on the magnitude of Q_{perp}. Even for arbitrary compact atomic surfaces, this will be true for small Q_{perp}. The partial structure factors in figure 6 fall nicely onto two smooth curves for $Q_{perp} < 0.4$, which demonstrates that (i) the SP model is a useful starting point, (ii) the overall extraction procedure of the partial structure factor is valid, and (iii) the lattice formed by Pd atoms is strongly FCC rather than the superlattice observed in the raw data. Similar results on the approximate position of Cu atoms (analogous to Pd atoms)

have been obtained on powder samples in the AlCuRu [71] and AlCuFe [72] icosahedral phases, although far fewer reflections were involved.

Looking at the Q_{perp} dependence of the partial structure factor, it is tempting to perform a phase reconstruction. In effect we observe an oscillating function, and since the quasicrystalline structure is centrosymmetric, only a plus or minus sign has to be attributed to the partial structure factor. The phase reconstruction was done in the following way.

(i) N and M have the same parity, (figure 6 (top)): F_{Pd} is positive for Q_{perp} lower than 0.5 or larger than 1, otherwise it is negative.

(ii) N and M have opposite parity, (figure 6 (bottom)): F_{Pd} is positive for Q_{perp} lower than 0.4 or greater than 1, otherwise it is negative.

Obviously one does not expect this phase reconstruction to be completely rigorous, especially in the large-Q_{perp} region, but at least 80% of the phases should be determined correctly (i.e. in regions of figure 6 where the oscillation is clearly visible). This can give an insight into the local structure to guide further modelling. The 6D density map shows only two features located at n_0 and bc_1. The shape of both atomic surfaces is mainly spherical, with very little faceting, which is rather a disappointment. This is certainly to be attributed to the severe truncation effects occurring. However, when looking at the density profile of the n_0 atomic surface, one find a qualitative agreement with the previously proposed SP model, i.e., Pd atoms are located on a spherical shell. The centre part is occupied by Mn atoms, whereas the outer part will be enclosed in an Al shell. The bc_1 site has mainly a spherical shape and contains only a small proportion of the Pd atoms. The shape and size of the density profile is smooth and in agreement with the SP model once truncation effects have been accounted for [73].

Both the Patterson map and the density map show atomic surfaces with a spherical shape. This makes any further modelling with faceted objects extremly difficult. It is clear from the Q_{perp} dependence of the partial structure factor that the spherical model is incorrect, for degenerate reflections (having the same value of Q_{perp} but belonging to different orbits) do not have the same structure factor. Such anisotropy can only be reproduced by more complex atomic surfaces, with the possible addition of some small 'parallel' component [74]. Moreover for the n_0 Pd shell, constraints on unphysically short distances (i.e. interatomic distances shorter than 2.3 Å) are extremely weak contrary to what occurs for the external shell of Al atoms. This makes the field of possible solutions extremely large, and precludes the proposition of a less crude model as was possible in the AlLiCu case for instance [13]. We will thus restrain ourselves to the comparison of the data with the SP model and try to extract some further useful information.

It is more informative to compare the data and model in reciprocal space. The solid lines in figure 6 represent the calculated Pd structure factor of the SP model. The data fall significantly below the SP model for high-Q_{perp} reflections. This observation leads us to consider bounded fluctuations of the atomic surfaces in perpendicular space. Such random phason disorder does not affect the long-range order of the structure so Bragg peaks are still observed, but their intensities are affected by a phason Debye–Waller term. The observed structure factors should be written

$$F_{obs} = F_{ideal} \exp(-B_{perp} Q_{perp}^2) \tag{8}$$

where F_{ideal} stands for the ideal structure without phason disorder. As a first approximation, we may say that it corresponds to the SP model. Now, plotting $\ln(F_{obs}/F_{ideal})$ against Q_{perp}^2 should show a linear decay. This is actually observed in figure 7, which demonstrates a

fairly clear trend with $B_{perp} = 1.35$ Å^2. Note that the deviations from a straight line in figure 7 are strongest near the nodes of the SP model prediction, where the data points have greater statistical errors. $B_{perp} = 1.35$ Å^2 is also obtained by fitting the F_{Pd} data to the modified SP model when an overall B_{perp} is introduced as a free parameter, with the important result that the fitted R factor improves from 50% to 20%.

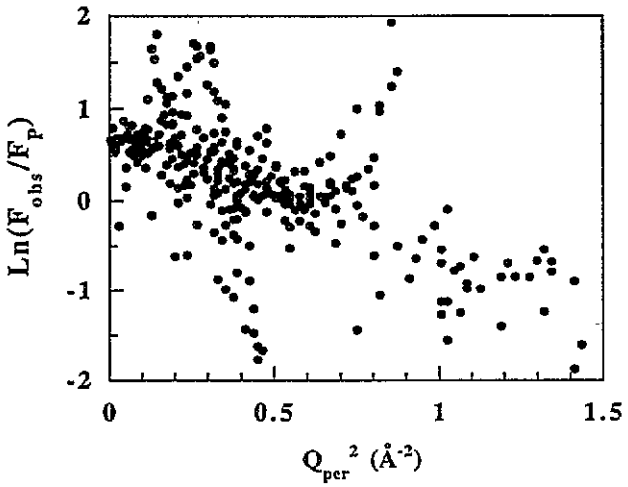

Figure 7. $\ln(F_{obs}/F_{SP})$ as a function of Q^2_{perp} for the experimental Pd partial structure factor. There is linear dependence, corresponding to a B_{perp} value of 1.35 Å^2.

What is the physical meaning of this perpendicular Debye–Waller factor? The above B_{perp} determination is strongly dependent on the model used as a reference, here the SP model. In particular, the analysis presented so far cannot distinguish a diffuse atomic surface due to phason fluctuations (called B^{rand}_{perp}) from a more complex, non-spherical atomic surface. In that case, our B_{perp} term would be a measure of departure of the 'true' atomic surface shape from sphericity (called B^{geom}_{perp}). We show in the following that both terms contribute.

5. Evidence for diffuse scattering

One clear signature of phason disorder would be diffuse x-ray scattering with an integrated intensity comparable to what is lost in the phason Debye–Waller factor. This has not been detected directly; however, we can see evidence for such phason diffuse scattering in comparison of high-resolution measurements of the Bragg intensity with low-resolution experiments, which integrate a significant fraction of the diffuse intensity. For this purpose, we use the total Bragg intensity from the present synchrotron results (away from the Pd edge, $\lambda = 0.54$ Å) and previous measurements performed on a standard x-ray tube (Mo Kα, $\lambda = 0.7$ Å). The volume of reciprocal space integrated with a low-resolution x-ray tube experiment is about three orders of magnitude larger than what is obtained with the synchrotron so that part of the diffuse scattering located close to the Bragg reflections is integrated. Indeed when x-ray tube data are compared to the SP model they do not show any Q_{perp} dependence as is the case with synchrotron data. That the diffuse intensity is related to random phason disorder can be shown by plotting $\ln(F_{sync}/F_{tube})$ as a function

of Q^2_{perp}. F_{sync} and F_{tube} stand for structure factors measured on the synchrotron (high resolution) and with an x-ray tube (low resolution). As shown in figure 8, there is a clear linear decrease which shows the existence of excess intensity in F_{tube} proportional to $F_{sync}[\exp(B_{perp}Q^2_{perp}) - 1]$, where B_{perp} is a perpendicular Debye–Waller factor. We find a perpendicular Debye–Waller factor, B_{perp}, equal to 0.7 Å^2, implying an RMS fluctuation of the atomic surfaces in perpendicular space equal to 1.2 Å. We stress that the two sets of data (each with 330 reflections), except the phason Debye–Waller term, are perfectly consistent. In particular Q_{perp} anisotropies of the structure factor, which are correlated to the details of the atomic surfaces, are identical in both cases. This is demonstrated by figure 9, where the high-resolution data measured and corrected for an overall perpendicular Debye–Waller factor are compared to the data obtained on the standard x-ray tube: note the very good agreement in the high-Q_{perp} region where the two data sets follow the same trend. The weighted R factor of agreement between the two data sets is 10% when the phason Debye–Waller factor is considered, compared to 20% when the B_{perp} correction is not carried out. This is also visible in figure 8, where the large majority of the 330 points lie very close to a straight line, with fluctuations well below 10%. This diffuse scattering demonstrates the existence of random fluctuations in perpendicular space of the atomic surfaces describing the atomic structure of the present AlPdMn icosahedral phase.

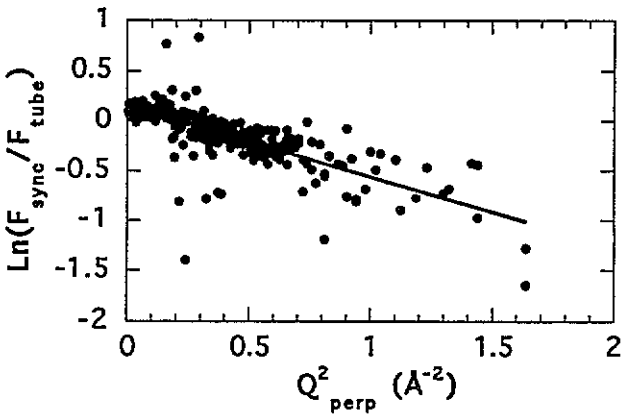

Figure 8. $\ln(F_{sync}/F_{tube})$ as a function of Q^2_{perp}. There is a linear decrease corresponding to a Q_{perp}-dependent diffuse scattering.

Further work, such as a direct determination of the shape of the diffuse scattering and its temperature dependence, is required to determine to which phenomenon it corresponds. The diffuse scattering can result from a random tiling type phase ('unlocked phase'), from isolated phason defects ('locked phase'), or from a phase transition. Indeed isolated phason defects would also give rise to a phason Debye–Waller decrease of the intensity. However, in that case, the diffuse scattering should be broad and extend far away from the Bragg reflection [49], whereas in a random tiling model the diffuse scattering is located close to the Bragg reflections and decreases as $1/k^2$ [42, 46]. Finally the phase diagram in the vicinity of the icosahedral i-AlPdMn phase is complex. In particular there exist a modulated icosahedral phase with a composition very close to the icosahedral one; it presents satellite reflections along the threefold axes [75]. Similarly to what has been observed in the i-AlCuFe modulated phase [76, 77] it seems that the modulation is related to a phason sine

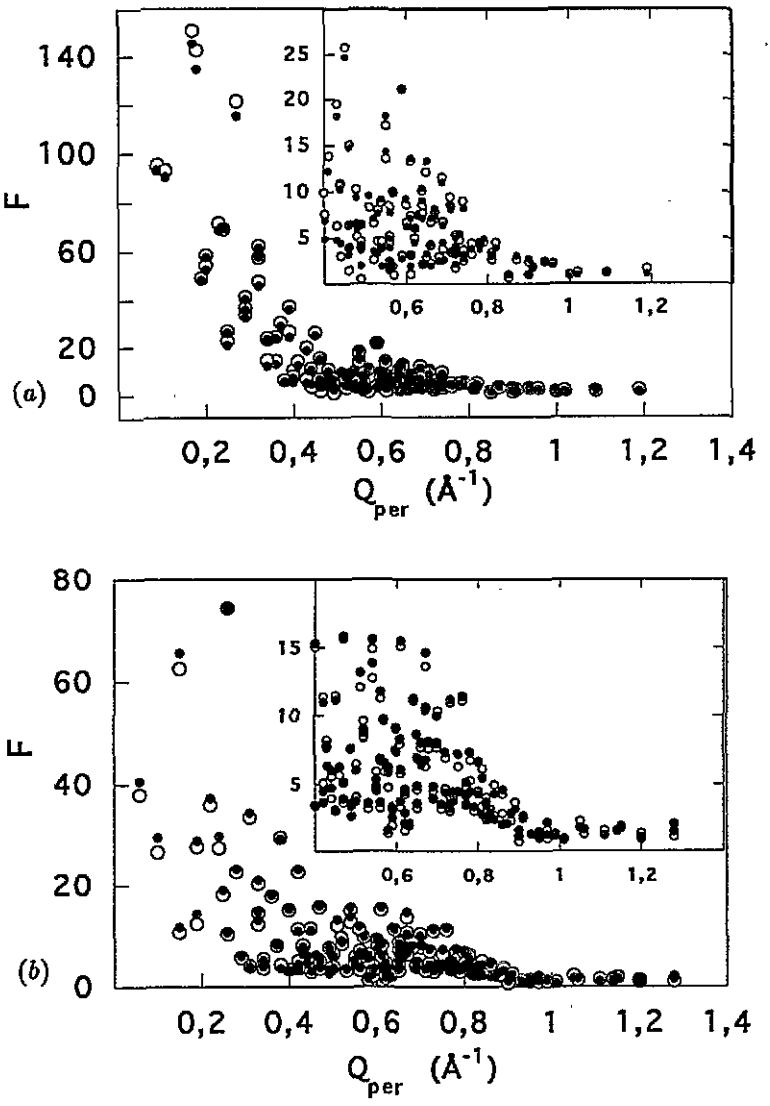

Figure 9. Comparison of the synchrotron data (open circles), once corrected for a perpendicular Debye–Waller factor with the x-ray tube data (filled circles). (a) is for P reflections and (b) for S reflections. The two data sets show the same anisotropy as a function of Q_{perp}, even in the high-Q_{perp} region (inset).

wave [78]. A precursor to this modulated phase could also give rise to diffuse scattering scaling with Q_{perp}.

If one assumes that all the diffuse scattering has been integrated with the low-resolution data, one can conclude that the partial Pd structure factor Q_{perp} decay contains two comparable contributions: the first is the result of random phason disorder (B_{perp}^{rand}), and the second must be reproduced by the precise geometry of the atomic surface which is certainly not a spherical shell or a sphere (B_1^{geom}). The geometrical roughness is of order 1.2 Å, to be compared to the spherical shell thickness equal to 2.8 Å ($R_1 = 5.35$ Å, $R_2 = 8.12$ Å). This suggests that the node Pd atomic surface is strongly stellated, or even

made of several disjointed pieces.

In order to evidence possible anisotropy of the node Pd atomic surface we have looked for anisotropy of the perpendicular Debye–Waller factor, in particular along high-symmetry directions, when comparing the data and the SP model [79]. Such a comparison did not show any significant differences: the three perpendicular Debye–Waller factors were found to be identical when using the (small) subset of data of reflections along a twofold, threefold, and fivefold axis. However one should note that there are very few reflections along these symmetry axes, which makes the comparison difficult. This is fairly consistent with figure 7 where the majority of the points lie quite close to a straight line, and where possible anisotropies are small. This fairly well rules out strongly stellated polyhedra and we conjecture that in order to reproduce the observed geometrical roughness the node Pd atomic surface is made of several disjointed pieces.

This raises the question of the precise modelling of the atomic surfaces. Let us consider the comparison of the present study with ideal and random-tiling-like models.

The volume found for the bc_1 Pd atomic surface is significantly larger than what is proposed in the AlCuFe case [28, 29]: in that work, the external shell of the atomic surface located in bc_1 is a triacontahedron τ times smaller than the standard one, whereas the external shell located at n_0 is a triacontahedron τ times larger than the standard one, and truncated along the fivefold axis to avoid short distances. In our result the volume of the bc_1 site is directly proportional to the difference between the low-Q_{perp} limit of the two curves shown in figure 6, and is significantly larger than the small triacontahedron ($V = 402$ Å^3 instead of 281 Å^3). The size of the bc site cannot be increased without a serious diminution of the atomic density. A possible solution would be to add small atomic surfaces on mid-edges, in the elongation of the bc_1 site. It has recently been pointed out that these small sites on mid-edges would hardly be seen on Patterson maps [80].

In order to evaluate the geometrical roughness of the other atomic surfaces, we also compared the SP model with the raw data measured close to the absorption edge where the scattering power of Pd atoms is smaller. As a free parameter a perpendicular Debye–Waller factors was introduced for each one of the six atomic surfaces. None of the perpendicular Debye–Waller factors could be neglected, for they significantly increased the agreement with the SP model. This was particularly true for the one associated with the Al atomic surface located at n_1 (note that there are practically only Al atoms on the site n_1). Similarly to the case of Pd atoms this perpendicular Debye–Waller factor contains both the geometrical and the random component, each one corresponding to RMS fluctuations of the order of 1 Å: this might also be an indication that the external shape of the n_1 atomic surface is more complex than the large triacontahedron as proposed in the Cornier-Quiquandon model.

The random phason fluctuation found here is of the order of a recent calculation of the phason fluctuation for a random tiling of canonical cells [81, 82]. However, the canonical cell model is based on chemically defined clusters of radius 10 Å (Mackay icosahedron), which put severe constraints on the Pd atomic surface shape. In particular, if Pd atoms are located precisely on the external shell of the Mackay icosahedron this would define its corresponding atomic surface. It is thus a crucial test to compare such a model with the present partial structure factor.

We have pointed out in section 1 the current difficulties of obtaining a satisfactory comparison between model and data. We conjecture that this is the result of an extremely complex shape of atomic surfaces, together with the occurrence of random fluctuations. That random fluctuations exist is not a serious problem since they can be incorporated in the modelling procedure similarly to what is done for thermal vibration. The complexity of the atomic surface shape is more serious. Unfortunately, because of truncation effects,

very little is learned when looking at the Patterson or density map. Because no constraint on short distances can be put forward for the Pd n_0 atomic surface, the field of possibilities is widely open and one needs either higher-Q_{perp} data or more efficient data treatment in order to proceed further in the modelling. A possibility is the use of the maximum entropy method for Fourier map calculation [83, 84]: this has been shown to be an efficient way of avoiding truncation effects. Another possibility, which partly avoids the truncation effect problem, is to perform a surface harmonic expansion of the atomic surface shape [85, 86]. Nevertheless the present partial structure factor data should simplify the atomic structure problem, since only one chemical species has to be considered.

6. Conclusion

Anomalous x-ray diffraction measurements with an AlPdMn single-grain quasicrystal have produced a reliable Pd partial structure factor†. We have shown that the comparison of a first-order model (SP model) with low-Q_{perp} data is a very efficient way of data renormalization. This technique could also be employed for partial structure factor determination of a large-unit-cell approximant, where the same kind of first-order model is in general easy to derive. The present measurements of the scattering amplitude from a single atomic species will make important contributions to the detailed determination of the atomic structure of a highly ordered quasicrystal. The very strong chemical order of Pd in the six-dimensional image of the structure has been shown unambiguously: the large majority of the Pd atomic surfaces definitively lie on n_0 and bc_1 sites only. In comparing the present high-resolution measurement with low-resolution data we have obtained strong experimental evidence for the existence of diffuse scattering located close to the Bragg reflections and whose intensity scales with $[1 - \exp(-B_{perp}Q_{perp}^2)]$, as expected from random fluctuations of the atomic surfaces in perpendicular space. The value of B_{perp} has been determined to be equal to 0.7 Å^2 corresponding to an RMS fluctuation of the atomic surfaces in perpendicular space equal to 1.2 Å. Moreover, a comparison with the SP model has shown that the geometrical irregularity of the atomic surface describing the Pd atoms is also of order 1 Å. This suggest that the Pd node atomic surface is built up from several disjointed pieces.

A determination of the origin of the diffuse scattering in the present perfect icosahedral phase (random tiling type phase, isolated phason defects, ...) requires further measurement of its shape and temperature dependence. This is in progress.

Acknowledgments

We are grateful to R Colella for the characterization of one of the samples, to S Kycia and A I Goldman for providing preliminary samples, and to A Darovsky and Y Gao for beam line support. We gratefully acknowledge useful discussions with P Kalugin, A I Goldman, R Colella, C Henley, M Mihalkovich, and M Oxborrow. The NSLS and the X17 wiggler beam line are supported by the US Department of Energy, Office of Basic Energy Sciences. The SUNY X3 Beamline at the NSLS is supported by the US Department of Energy under grant No DEFG-0291-ER45231. Work at Stony Brook was partially supported by the NSF under grant DMR-9202528. One of us (M de B) thanks the CNRS for financial support during his stay at SUNY, Stony Brook.

† Raw data are available from the authors upon request.

References

[1] Tsai A-P, Inoue A and Masumoto T 1987 *Japan. J. Appl. Phys.* **26** L1505
[2] Tsai A-P, Inoue A and Masumoto T 1988 *Japan. J. Appl. Phys.* **27** L1587
[3] Tsai A P, Inoue A, Yokoyama Y and Masumoto T 1990 *Mater. Trans. JIM* **31** 98
[4] Tsai A P, Inoue A and Masumoto T 1990 *Phil. Mag. Lett.* **62** 95
[5] Guryan C A, Goldman A I, Stephens P W, Hiraga K, Tsai A P, Inoue A and Masumoto T 1989 *Phys. Rev. Lett.* **62** 2409
[6] de Boissieu M, Durand-Charre M, Bastie P, Carabelli A, Boudard M, Bessiere M, Lefebvre S, Janot C and Audier M 1992 *Phil. Mag. Lett.* **65** 147
[7] Yokoyama Y, Tsai A P, Inoue A and Masumoto T 1991 *Mater. Trans. JIM* **32** 1089
[8] Yokoyama Y, Miura T, Tsai A P, Inoue A and Masumoto T 1992 *Mater. Trans. JIM* **33** 97
[9] Kycia S W, Goldman A I, Lograsso T A, Delancy D W, Sutton M, Dufresne E, Brüning R and Rodricks B 1993 *Phys. Rev.* B **48** 3544
[10] Janot C 1992 *Quasicrystals: A Primer* (Oxford: Oxford University Press)
[11] Janot C, Dubois J M and Pannetier J 1987 *Physica* B **146** 351
[12] Janot C, de Boissieu M, Dubois J M and Pannetier J 1989 *J. Phys.: Condens. Matter* **1** 1029
[13] de Boissieu M, Janot C, Dubois J M, Audier M and Dubost B 1991 *J. Phys.: Condens. Matter* **3** 1
[14] Shechtman D, Blech I, Gratias D and Cahn J W 1984 *Phys. Rev. Lett.* **53** 1951
[15] Elswijk H B, de Hosson J T M, van Smaalen S and de Boer J L 1988 *Phys. Rev.* B **38** 1681
[16] Yamamoto A 1992 *Phys. Rev.* B **45** 5217
[17] Gratias D 1994 *GDR 5 Quasicrystal Meeting (Saclay, 1994)*
[18] Kalugin P A, Kitaev A Y and Levitov L S 1985 *JETP Lett.* **41** 145
[19] Kalugin P A, Kitayev A Y and Levitov L S 1985 *J. Physique. Lett.* **46** L601
[20] Bak P 1985 *Phys. Rev.* B **32** 5764
[21] Lubensky T C, Ramaswamy S and Torner J 1985 *Phys. Rev.* B **32** 7444
[22] Lubensky T C, Socolar J E S, Steinhardt P J, Bancel P A and Heiney P 1986 *Phys. Rev. Lett.* **57** 1440
[23] Heiney P A, Bancel P A, Horn P M, Jordan J L, LaPlaca S, Angilello J and Gayle F W 1987 *Science* **238** 660
[24] Elser V 1985 *Phys. Rev. Lett.* **54** 1730
[25] Elser V 1985 *Phys. Rev.* B **32** 4892
[26] Kalugin P A 1989 *Europhys. Lett.* **9** 545
[27] Katz A 1990 *Number Theory and Physics* ed J M Luck, P Moussa, M Waldschmidt and C Itzykson (Berlin: Springer) p 100
[28] Cornier-Quiquandon M, Quivy M, Lefebvre S, Elkaim E, Heger G, Katz A and Gratias D 1991 *Phys. Rev.* B **44** 2071
[29] Katz A and Gratias D 1993 *J. Non-Cryst. Solids* **153&154** 187
[30] Gähler F 1988 *Doctoral Thesis* Swiss Federal Institute of Technology (ETH)
[31] Baake M, Klitzing R and Schlottmann M 1992 *Physica* A **191** 554
[32] Smith A P 1993 *J. Non-Cryst. Solids* **153&154** 258
[33] Elser V 1989 *Aperiodic Crystals* ed M V Jaric (Berlin: Academic) p 105
[34] Henley C L 1991 *Phys. Rev.* B **43** 993
[35] Henley C L 1991 *Quasicrystals: The State of The Art* ed D P DiVincenzo and P J Steinhardt (Singapore: World Scientific) p 429
[36] This is what C L Henley calls the 'maximally random tiling model'. When an energy cost is introduced for a phason jump, two phases can be distinguished. The first is the 'unlocked' phase or random tiling type phase in the high-temperature region. This phase has an entropy which varies as the squared gradient of the phason strain, similarly to the 'maximally random tiling model'. At lower temperature it is a 'locked' phase, with isolated phason defects. (See hereafter.)
[37] Lançon F, Billard L and Chaudari P 1986 *Europhys. Lett.* **2** 625
[38] Lançon F and Billard L 1988 *J. Physique* **49** 249
[39] Henley C L 1988 *J. Phys. A: Math. Gen.* **21** 1649
[40] Widom M, Deng D P and Henley C l 1989 *Phys. Rev. Lett.* **63** 310
[41] Strandburg K J, Tang L-H and Jaric M V 1989 *Phys. Rev. Lett.* **63** 314
[42] Tang L H 1990 *Phys. Rev. Lett.* **64** 2390
[43] Tang L H and Jaric M V 1990 *Phys. Rev.* B **41** 4524
[44] Oxborrow M and Henley C L 1993 *Phys. Rev.* B **48** 6966
[45] Widom M 1993 *Phys. Rev. Lett.* **70** 2094
[46] Jaric M V and Nelson D R 1988 *Phys. Rev.* B **37** 4458

[47] Mihalkovic M and Mrafko P 1993 *J. Physique* I **3** 687
[48] Mihalkovic M and Mrafko P 1993 *Europhys. Lett.* **21** 463
[49] Kalugin P 1993 unpublished result
[50] Jeong H C and Steinhardt P J 1993 *Phys. Rev.* B **48** 9394
[51] Dotera T and Steinhardt P J 1994 *Phys. Rev. Lett.* **72** 1670
[52] Audier M and Guyot P 1990 *Quasicrystals and Incommensurate Structures in Condensed Matter (3rd Int. Meeting on Quasicrystals (1989)* ed M J Yacaman *et al* (Beijing: World Scientific) p 288
[53] Audier M and Guyot P 1990 *Quasicrystal* ed M V Jaric and S Lundqvist (Singapore: World Scientific) p 74
[54] Janot C, Audier M, De Boissieu M and Dubois J M 1991 *Europhys. Lett.* **14** 355
[55] Coddens G, Bellissent R, Calvayrac Y and Ambroise J P 1991 *Europhys. Lett.* **16** 271
[56] Coddens G, Soustelle C, Bellissent R and Calvayrac Y 1993 *Europhys. Lett.* **23** 33
[57] Bresson L 1994 *Winter School on Quasicrystals (Les Houches, 1994)* ed D Gratias and F Hippert (Les Ulis: Editions de Physique)
[58] Kalugin P and Katz A 1993 *Europhys. Lett.* **21** 921
[59] de Boissieu M, Stephens P, Boudard M, Janot C, Chapman D L and Audier M 1994 *Phys. Rev. Lett.* **72** 3538
[60] Boudard M, de Boissieu M, Janot C, Dubois J M and Dong C 1991 *Phil. Mag. Lett.* **64** 197
[61] Boudard M, de Boissieu M, Janot C, Heger G, Beeli C, Nissen H-U, Vincent P, Ibberson R, Audier M and Dubois J M 1992 *J. Phys.: Condens. Matter* **4** 10 149
[62] Devaud-Rzepski J, Quivy A, Calvayrac Y, Cornier-Quiquandon M and Gratias D 1989 *Phil. Mag.* B **60** 855
[63] Coppens P 1992 *Synchrotron Radiation Crystallography* (New York: Academic)
[64] de Boissieu M, Stephens P, Boudard M and Janot C 1994 *J. Phys.: Condens. Matter* **6** 363
[65] Lee H, Collela R and Chapman L D 1993 *Acta. Crystallogr.* A **49** 600
[66] Lee H 1993 *Thesis* Purdue University
[67] Roth M, Lewit-Bentley A and Bentley G A 1984 *J. Appl. Crystallogr.* **17** 77
[68] Ice G E, Sparks C J and Habenschuss A 1992 *Phys. Rev. Lett.* **68** 863
[69] Kan X B, Robertson J L, Moss S C, Kulik J, Ishimasa T, Mori M, Quivy A, Gratias D, Elser V and Zschack P 1993 *J. Non-Cryst. Solids* **153&154** 33
[70] Cahn J W, Shechtman D and Gratias D 1986 *J. Mater. Res.* **1** 13
[71] Hu R, Egami T, Tsai A-P, Inoue A and Masumoto T 1992 *Phys. Rev.* B **46** 6105
[72] Cornier-Quiquandon M, Bellissent R, Calvayrac Y, Cahn J W, Gratias D and Mozer B 1993 *J. Non-Cryst. Solids* **153&154** 10
[73] de Boissieu M, Janot C and Dubois J M 1988 *Europhys. Lett.* **7** 593
[74] de Boissieu M, Janot C and Dubois J M 1990 *J. Phys.: Condens. Matter* **2** 2499
[75] Audier M, Durand-Charre M and de Boissieu M 1993 *Phil. Mag.* B **68** 607
[76] Menguy N, de Boissieu M, Guyot P, Audier M, Elkaim E and Lauriat J P 1993 *J. Physique* I **3** 1953
[77] Bancel P 1993 *Phil. Mag. Lett.* **67** 43
[78] de Boissieu M, Kycia S, Goldman A I, Boudard M, Janot C and Audier M unpublished results
[79] We thank one of the referees for this suggestion
[80] Boudard M, de Boissieu M and Janot C 1993 *Europhys. Lett.* **23** 181
[81] Newman M E J, Oxborrow M and Henley C L 1994 *Phil. Mag.* B
at press
[82] Newman M E J and Henley C L 1994 *Phys. Rev.* B submitted
[83] de Boissieu M, Papoular R J and Janot C 1991 *Europhys. Lett.* **16** 343
[84] Steurer W, Haibach T and Zhang B 1993 *Acta. Crystallogr.* B **49** 661
[85] Elcoro L, Perez-Mato J M and Madariaga G 1994 *Acta Crystallogr.* A **50** 182
[86] Elcoro L and Perez-Mato J M 1994 *Acta Crystallogr.* B **50** 294